Fast Korringa-Kohn-Rostoker coherent potential approximation and its application to FCC Ni-Fe systems

1989 J. Phys.: Condens. Matter 1 8045

(http://iopscience.iop.org/0953-8984/1/43/006)

J. Phys.: Condens. Matter 1 (1989) 8045–8063. Printed in the UK

Fast Korringa–Kohn–Rostoker coherent potential approximation and its application to FCC Ni–Fe systems

H Akai†

Department of Physics, Nara Medical University, Kashihara, Nara 634, Japan

Received 24 April 1989

Abstract. A fast KKR CPA method is explained and its convergence properties are examined numerically. It is shown that a step number of $N \simeq 300$, which determines the number of k-points used for the numerical integration in the k-space as well as the number of iteration steps in determining the coherent t-matrix, is sufficient for most purposes, including total-energy calculations. As a typical application the electronic structure of ferromagnetic Ni–Fe systems is calculated in the framework of the KKR CPA combined with the local spin density approximation, which demonstrates the feasibility of the present method.

1. Introduction

The coherent potential approximation within the Korringa–Kohn–Rostoker band structure scheme (KKR CPA) was first proposed by Shiba [1] and by Soven [2] and represents the most sophisticated method to treat the electronic structure of disordered alloys. In the past, many efforts have been made to apply it to real alloy systems. In particular, the success of the local spin density approximation (LSD) in the studies of the cohesive properties of pure metals [3] was a strong motivation to investigate disordered alloy systems on an equally sound basis as the pure systems. However, due to enormous numerical problems, such an attempt, called KKR CPA LSD, has been undertaken only for very few systems [4–10] despite the fact that its efficiency is now well recognised.

The main reason for this lies in the numerical difficulties in solving the KKR CPA. To make this point clearer let us first look at the KKR CPA formalism briefly. The average properties of disordered systems are described by the coherent t-matrix $t(E)$ which is determined self-consistently in the following way. Consider the on-the-energy-shell part of the t-matrix $T(E)$ of the system (so-called scattering path operator):

$$T(E) = \frac{1}{\tau} \int_{\tau} \mathrm{d}^3k \, [t^{-1}(E) - G_0(\boldsymbol{k}, E)]^{-1}. \tag{1.1}$$

Here the k-space integral is performed over the first Brillouin zone (BZ) of volume τ. $G_{0LL'}$ is the structural Green function of the KKR band structure method. The self-consistent condition determining $t(E)$ is now written as

$$c_{\mathrm{A}}(t_{\mathrm{A}}^{-1} - t^{-1} + T^{-1})^{-1} + c_{\mathrm{B}}(t_{\mathrm{B}}^{-1} - t^{-1} + T^{-1})^{-1} = T \tag{1.2}$$

† Part of this work was performed during repeated stays by the author at Institut für Festkörperforschung der Kernforschungsanlage Jülich, D5170 Jülich, Federal Republic of Germany.

0953-8984/89/438045+19$02.50

where A or B denote the atomic species, and c_A (c_B) and t_A (t_B) are the concentration and the t-matrix of the single muffin-tin potential of the A (B) atom, respectively. Since t is unknown initially we have to determine it iteratively. Starting from a trial value of t, we perform the k-space integration and see if the self-consistency condition is fulfilled. If it is not, we calculate an improved t from (1.2) and repeat the whole process over and again until self-consistency is achieved. Since all the quantities in the expression are matrices, e.g., of rank 9×9 if angular momenta up to $l = 2$ are taken into account, and moreover energy dependent, the k-space integral appearing in (1.2) represents the real troublesome problem. Typically in order to achieve self-consistency within the sense of CPA and LSD the BZ integral has to be calculated about 10^5 times. Therefore a KKR CPA LSD calculation, performed in this way, will cost hundred times more computation time than a usual KKR band structure calculation.

However, because of, firstly, general development of computers, especially the availability of supercomputers, and, secondly, several techniques which greatly improve the efficiency of the computation without sacrificing the accuracy too much [11–15], KKR CPA LSD calculations become just feasible. It is in reality now a rather inexpensive kind of computation.

This article attempts to explain a fast KKR CPA method in detail. One of the key points of our fast KKR CPA is the k-space integration [11, 12] which is performed step by step in parallel with the self-consistent determination of the coherent t-matrix. Though the method was proposed many years ago [11] and also has been used by the present author [4, 5, 9–12], its efficiency has not been well understood since details have not been published. Therefore it is worthwhile to demonstrate how it works and to examine the convergence properties of the procedure critically to establish it as a method.

In addition to the method of the k-space integration mentioned above, we also employ some other techniques which are efficient not only for KKR CPA but also for more general electronic structure calculations. With all these techniques, together with the vectorisation for the supercomputers, really fast computation is now accessible; surprisingly, it runs much faster than our linearised version (LMTO) of the KKR band structure calculation.

Section 2 is devoted to explain our fast KKR CPA technique. The convergence of the k-space integration employed in the actual use of this technique is fully examined in §3. Section 4 presents, as an example, the result of KKR CPA LSD calculations for FCC Ni–Fe systems. Since all the quantities, including the lattice constant, are determined from first-principles so as to minimise the total energy, they are analogous to and should have a similar predictive power as the most elaborate version of the KKR band structure calculations in the case of ordered systems. We summarise in §5.

2. Fast KKR CPA method

2.1. KKR CPA

We first briefly outline the KKR CPA method to make clear in what we will concern ourselves hereafter. For details, we refer to [12] and the references given therein. The Hamiltonian for the Kohn–Sham equation of a given substitutional alloy $A_{1-x}B_x$ is assumed to be in atomic unit

$$H = -\nabla^2 + V(\boldsymbol{r}) \tag{2.1}$$

where $V(\boldsymbol{r})$ represents an assembly of muffin-tin potentials. The Green function of the system can be written in a cell-centered representation as

$$G(\boldsymbol{r}+\boldsymbol{R}_i,\boldsymbol{r}'+\boldsymbol{R}_j;E)=G_i^{\mathrm{s}}(\boldsymbol{r}+\boldsymbol{R}_i,\boldsymbol{r}'+\boldsymbol{R}_j;E)\delta_{ij}+G^{\mathrm{b}}(\boldsymbol{r}+\boldsymbol{R}_i,\boldsymbol{r}'+\boldsymbol{R}_j;E) \tag{2.2}$$

where in each cell G_i^{s} is the Green function for the single muffin-tin potential in free space and G^{b} represents the multiple scattering contribution ('back scattering'). Since the imaginary part of the first term G_i^{s} can easily be calculated if the radial wavefunction for the single potential is known, our main interest focused on the second term G^{b}, which is double expanded into radial eigenfunctions of the local muffin-tin potentials:

$$G^{\mathrm{b}}(\boldsymbol{r}+\boldsymbol{R}_i,\boldsymbol{r}'+\boldsymbol{R}_j;E)=\sum_{LL'}Y_L(\hat{\boldsymbol{r}})J_{li}(r,E)B_{Li,L'j}(E)Y_{L'}(\hat{\boldsymbol{r}}')J_{l'j}(r',E). \tag{2.3}$$

Here $Y_L(\hat{\boldsymbol{r}})$ is the spherical harmonics of angular momentum $L=(l,m)$ and J_{li} is the radial wave function with angular momentum l for the muffin-tin potential at the ith site. $J_{li}(r)$ is regular at the origin and is normalised such that it coincides with

$$j_l(\sqrt{E}r)+\sqrt{E}t_{li}(E)h_l(\sqrt{E}r) \tag{2.4}$$

outside the muffin-tin sphere $r>r_{\mathrm{mt}}$. Here j_l and h_l are the spherical Bessel and Hankel function ($h_l=n_l-ij_l$; n_l is the spherical Neumann function), respectively, and $t_{li}(E)$ is the atomic t-matrix for the muffin-tin potential, $t_{li}(E)=(-1/\sqrt{E})\sin\eta_{li}\exp(i\eta_{li})$ ($\eta_{li}(E)$: phase-shift).

In the CPA, as mentioned in §1 the average properties of the system are described by the coherent t-matrix t which is determined self-consistently in the sense of the mean field theory. We first consider an A or B atom with single site potential V_{A} or V_{B} embedded in an otherwise perfect crystal. The host atoms are now the effective atoms specified by the coherent t-matrix t. This is the single-site impurity problem and is solved by a standard method [16–20]. Suppose A or B atoms are located at the origin. The back-scattering part B_i ($i=$ A or B) of the Green function G_i for the perturbed system is calculated from the corresponding unperturbed Green function B as

$$B_i=B[1-B(t_i-t)]^{-1} \qquad i=\text{A or B} \tag{2.5}$$

where B is given by

$$B=-t^{-1}+t^{-1}Tt^{-1}. \tag{2.6}$$

Here T is the on-the-energy-shell part of the site-diagonal t-matrix of the averaged whole system given by (1.1). Now the self-consistent equation determining t is

$$c_{\mathrm{A}}B_{\mathrm{A}}+c_{\mathrm{B}}B_{\mathrm{B}}=B \tag{2.7}$$

which is equivalent to the condition given by (1.2).

In the following we discuss how to solve the self-consistent equations ((1.1) and (1.2)) fast enough so as to ensure that a sufficient number of iterations needed for the LSD self-consistency can be carried out in reasonable computing time.

2.2. k-space integration

As was mentioned in §1, we perform the k-space integration and the self-consistent determination of the coherent t-matrix simultaneously [11] to overcome the main difficulty arising in KKR CPA. For brevity we consider a cubic crystal and take a set of k-points $\{\boldsymbol{k}_n\}$ which distribute in $\frac{1}{48}$ of the first Brillouin zone following Weyl's uniform distribution [22]:

$$\begin{aligned} k_{nx} &= n\xi_x - [n\xi_x] \\ k_{ny} &= n\xi_y - [n\xi_y] \qquad n = 1, 2, \ldots \\ k_{nz} &= n\xi_z - [n\xi_z] \end{aligned} \tag{2.8}$$

where ξ_x, ξ_y and ξ_z are irrational numbers with the ratio between them being also irrational, and $[\ldots]$ denotes the integer part. Here we take the unit of the k-vector such that the zone boundary in [100], [010] and [001] directions lies on $k_x = 1$, $k_y = 1$ and $k_z = 1$ planes. Also any $\boldsymbol{k}_n$ which falls outside the $\frac{1}{48}$ Brillouin zone must be omitted from the series. Such distribution satisfies Weyl's criterion of uniform distribution:

$$\lim_{N\to\infty} \frac{1}{N} \sum_{n=1}^{N} f(\boldsymbol{k}_n) = \frac{1}{\tau} \int_{\tau} f(\boldsymbol{k})\, \mathrm{d}^3k \tag{2.9}$$

where $f(\boldsymbol{k})$ is a Riemann integrable function. A similar relation holds also for a random distribution. However, the convergence of the LHS of (2.9) with Weyl's uniform distribution is far faster than the so-called Monte Carlo integration based on a complete random selection of k-points. Actually the convergence rate of the LHS of (2.9) is $1/N$ instead of $1/\sqrt{N}$ which is expected for the Monte Carlo integration. In the following we fix ξ to $(\sqrt{3}a, \sqrt{5}a, 2\sqrt{13}a)$ with $a = 0.359$ so as to ensure that our results are exactly reproducible. For finite N the result of the sum, as a matter of course, depends on the choice of the vector ξ, especially for small N (typically for $N < 50$). Though we have no strict criterion for the choice of ξ, it certainly is desirable from the view point of the self-consistent determination (see below) of the coherent t-matrix that the sum, as a function of N, does not deviate too much from its limiting value even for small N. This can be partly attained by optimising ξ for several test cases. The present value for ξ is one of those chosen after such optimisation.

The basic idea of our method is to make use of (2.9) with finite N as an approximate expression for an integral. Starting from small N, say $N \simeq 1$–10, and a trial value for t we can *continuously* improve the evaluation of (1.1) of §1 by increasing N, i.e., adding additional k-points to the integration without recalculating the previous ones, and modifying t simultaneously and successively. The actual iteration process for the matrices T and t can be written down shortly as

$$T_n = (1 - 1/n)\, T_{n-1} + (1/n)\, [t_n^{-1} - G_0(\boldsymbol{k}_n)]^{-1} \tag{2.10}$$

and

$$c_{\mathrm{A}}(t_{\mathrm{A}}^{-1} - t_n^{-1} + T_n^{-1})^{-1} + c_{\mathrm{B}}(t_{\mathrm{B}}^{-1} - t_n^{-1} + T_n^{-1})^{-1} = [\gamma\,(t_{n+1}^{-1} - t_n^{-1}) + T_n^{-1}]^{-1} \tag{2.11}$$

with γ ($\gamma \geq 1$) being a parameter for optimising the convergence of the procedure. An alternative of (2.11) is

$$c_{\mathrm{A}}(t_{\mathrm{A}} - t_n - B_n^{-1})^{-1} + c_{\mathrm{B}}(t_{\mathrm{B}} - t_n - B_n^{-1})^{-1} = [\gamma\,(t_{n+1} - t_n) - B_n^{-1}]^{-1} \tag{2.12}$$

where B_n is related to T_n (and t_n) through (2.6). Note that (2.11) and (2.12) are equivalent *only* when $\gamma = 1$ and hence, in general, should show different behavior as iteration schemes.

Since the coherent t-matrix t_n is now dependent on n, (2.10) is not a direct application of Weyl's criterion, (2.9), to the integral given by (1.1). However, it is easily shown that, if T_n and t_n converge towards values T_∞ and t_∞ for large n, those values also satisfy the original self-consistent equation given by (1.1) and (1.2). The important point is that the convergence is usually fast, especially when the random scattering is strong.

As a starting value for t we usually choose

$$t = \begin{cases} (c_A t_A^{-1} + c_B t_B^{-1})^{-1} & \text{for d states} \\ c_A t_A + c_B t_B & \text{for others.} \end{cases} \tag{2.13}$$

Correspondingly we use (2.11) for d states and (2.12) for s and p states as an iteration scheme. This, however, is not a strict rule. For example, if there exists a resonance, say, in the p states, the first alternative for t_p will give a better convergence. On the other hand, for non-transition metal alloys for which t_d can be small the second one may be adequate even for d states. In any case we should try these possibilities, especially when the convergence is not so smooth or even it diverges.

We also adjust γ to improve the convergence. A value between 2 and 20, depending both on l (s,p,d,...) and on the condition (resonance, off-resonance, split-band, etc.), usually gives good results. Though a bigger γ provides slower but smoother convergence, too big a value for γ should be avoided; it may cost too much computer time before a good convergence is attained.

It sometimes happens that the starting values for t are so poor that they make rather unrealistic contributions to the integral. Though the process mostly converges even in such cases, the convergence will be generally improved by getting rid of the bad history of the early steps. This is realised by implementing a weighting factor to each sum:

$$T_n = (1/S_n)\{S_{n-1} T_{n-1} + w_n [t_{n-1} - G_0(\boldsymbol{k}_n)]^{-1}\} \tag{2.14}$$

with

$$S_n = S_{n-1} + w_n. \tag{2.15}$$

Here w_n is chosen, for instance, as

$$w_n = 1 - \alpha^n. \tag{2.16}$$

The procedure shown here with $\alpha \simeq 0.99$ usually works efficiently as will be shown in §3.

Sometimes, though not so often, it can happen that none of the above tricks help and the procedure diverges. One way to avoid such a difficult situation is to shift the energy origin for the structural Green function. Such shift of the energy origin are possible in the sense of the atomic sphere approximation (ASA) of Andersen [23] because the energy zero is arbitrary in this approximation. We can also use this approximation for the muffin-tin potential by introducing a hypothetical atomic sphere

which contains both the muffin-tin and interstitial regions. The atomic t-matrix is then evaluated at this atomic sphere, not at the muffin-tin sphere as it is usually done.

In this case the atomic t-matrix rigorously depends on a choice of the energy origin. The final results, nevertheless, should be very insensitive; only small inconsistencies brought in either by the ASA or by the truncation of the angular momentum in the KKR-matrix would be responsible for any residual dependence. We can make use of this invariance to improve the convergence. For example, if t_i^{-1} (i = A or B) diverges for certain energy, as is often seen for sp metals, it may be helpful to shift the energy origin of the structural Green function by Δ such that the pole falls outside the energy region of interest.

A more elaborated way is to use an energy-dependent shift $\Delta(E)$, which originally was introduced to eliminate the energy dependence of the structural Green function for the LMTO scheme by Andersen [23]. For the present purpose the energy dependence of $\Delta(E)$ can be rather arbitrary and we employ it when a fixed Δ is not enough to remove all of the poles or anything which causes difficulties. Thus required shifts are typically 0.1–0.2 Ryd; such a shift practically does not affect the final result (e.g., the equilibrium lattice constant changes around 0.1% in Fe alloy cases) despite the inconsistency inherent in the ASA, but ensures a fast and smooth convergence. We notice, however, that using the ASA clearly introduces an additional approximation to the CPA, and hence, should better be avoided as long as possible.

2.3. Energy integration

Once the Green function G_i (i = A or B) is known the local charge or spin density is calculated by integrating the Green function for each spin direction up to the Fermi level:

$$\rho_i(\boldsymbol{r}) = \frac{1}{\pi}\,\mathrm{Im}\int_{-\infty}^{E_\mathrm{F}} \mathrm{d}E\,\left(G_i^{\mathrm{s}}(\boldsymbol{r},\boldsymbol{r}\,;E) + G_i^{\mathrm{b}}(\boldsymbol{r},\boldsymbol{r}\,;E)\right). \tag{2.17}$$

Since both G_i^{s} and $G_i = G_i^{\mathrm{s}} + G_i^{\mathrm{b}}$ are Green functions and as such analytic as a function of the complex energy E in the upper complex half plane, the same is also true for G_i^{b}. We can, therefore, deform the integration path into the upper half plane [21], which greatly improves the accuracy of the integration since $G_i^{\mathrm{b}}(\boldsymbol{r},\boldsymbol{r}\,;E)$ is quite structureless for E apart from the real axis. On the other hand, G_i^{s} is integrated for convenience along the real axis, since in this case only the regular solution of the radial wavefunction J is needed. Otherwise we also need the irregular solution which is more difficult to calculate. Using the expression for the Green function of a single muffin-tin potential, we calculate the first term of the RHS of (2.17) as

$$-\frac{1}{\pi}\,\mathrm{Im}\int_{-\infty}^{E_\mathrm{F}} \mathrm{d}E\,G_i^{\mathrm{s}}(E) = \frac{1}{\pi}\int_{-\infty}^{E_\mathrm{F}} \mathrm{d}E\sum_L Y_L^2(\hat{\boldsymbol{r}})J_{li}^2(r,E)\sqrt{E}. \tag{2.18}$$

To perform these energy integrations, we have to calculate radial wavefunction $J(r,E)$ by solving the Schrödinger equation on each energy mesh point. Moreover, these energies are complex in the present scheme. Though not many mesh points, typically 30–40, are needed for the integration of G_i^{b}, it is still desirable to decrease the number of the energy points for which we have to solve the Schrödinger equation.

A simple way to realise this is to expand the energy dependence of the normalised radial wavefunction $\tilde{J}(r,E) = \Omega(E)J(r,E)$ into the Chebyshev polynomials. Here Ω is

a energy dependent normalisation constant and the normalisation is

$$\int_0^{r_{mt}} r^2 \mathrm{d}r |\tilde{J}(r,E)|^2 = 1. \tag{2.19}$$

(Such normalisation is necessary because $J(r,E)$ itself is not a smooth function of the energy, especially near a resonance.) Now we expand $|\tilde{J}|^2$ (rather than $\tilde{J}$ itself, for convenience) in a given energy interval $E_1 < E < E_2$ as

$$|\tilde{J}(r,E)|^2 = \sum_{i=0}^{n} A_i(r)\, T_i(\epsilon) \tag{2.20}$$

where the T_n are the Chebyshev polynomials of nth order, the $A_n(r)$ are expansion coefficients and ϵ is defined by $\epsilon = (2E - E_2 - E_1)/(E_2 - E_1)$. The energy integrations are then performed on $T_i(\epsilon)\, B(\epsilon)$ $(i = 1,\ldots,n)$ for the 'back-scattering' terms and the corresponding ones for the single-potential terms. Since the polynomials are analytic, the expansion on the real axis is sufficient even for the complex energy integral. These integrals define a series I_i $(i = 1,\ldots,n)$ which contains the imaginary part of the integrals related to T_i. Expansion coefficients $A_i(r)$, on the other hand, are expressed as

$$A_i(r) = \sum_{j=0}^{n} W_j\, T_i(\epsilon_j)\, |J(r,\epsilon_j)|^2 \tag{2.21}$$

where the ϵ_j are given by

$$\epsilon_j = \cos\left(\frac{2j+1}{n+1}\frac{\pi}{2}\right) \qquad j = 1,\ldots,n \tag{2.22}$$

and the W_j are weighting factors: $W_j = 1/(n+1)$, if $j = 0$; $W_j = 2/(n+1)$, otherwise. By use of these expression the charge (or spin) densities are obtained in the form

$$\rho(r) = \sum_{j=0}^{n} |J(r,\epsilon_j)|^2 \sum_{i=0}^{n} W_j\, T_i(\epsilon_j)\, I_i. \tag{2.23}$$

Since the r-dependent expansion coefficients $A_i(r)$ do not enter the final expression (2.23), it obviouly is not necessary to evluate (2.21). The second summation term of (2.23) simply gives a weight to the radial wavefunction at the energy ϵ_j. Since the Chebyshev expansion up to $n \simeq 8$–10 is sufficient for an energy interval around 2 Ryd, it considerably reduces the computational work. Moreover, it enables us to perform the complex energy integral with *real energy* wavefunctions and also gives a compact and transparent way of calculating the charge densities.

2.4. Vectorisation

In our fast KKR CPA method, each k-point does not contribute independently to the final result because the first k-point modifies a given coherent t-matrix and thus affects the result by the second k-point, and so on. For this reason the process cannot directly be vectorised. However, if we form the k-points into bunches such that each of them contains a certain number of k-points, we can vectorise the procedure by using a

fixed coherent t-matrix within the bunch. It is also clear that each energy contributes independently in the procedure, and hence, is vectorised.

We usually bunch 9 k-points with 39 complex energies. The whole procedure is then vectorised with vectors of length 351 (9×39), long enough to derive full advantage of the vector processing. We must take care, however, that every step of the procedure should work on these vectors. For example, matrix inversion in (2.10) is taken not by vectorising the column or row vectors of the matrix but by dealing with each element as a vector, since it really is. With such care an acceleration by a factor of 30–40 is rather easily attained; typical computing times with 500 k-points are about 1 s on NEC SX-2N (1 processor, 4 multi-parallel-pipelines), around twice as much on CRAY X-MP/22 (2 processors, but likely single-tasking), for one LSD iteration cycle (i.e., the CPA iteration for all energies and spins with the construction of charge/spin densities).

3. Convergence properties

Whether our iteration procedure is practical or not depends on how fast the numerical integration of (2.9) converges. Probably the worst case is the pure limit, where for concentrations c_A or $c_B = 0$ the integrand becomes singular for real energies. Though we can mostly avoid these singularities by introducing the complex energy integration, the treatment at the Fermi level is somehow a problem. We usually retain a small but finite imaginary part, typically 10^{-4} (in atomic units), to the Fermi level in order to remove the singularity. For such a small imaginary part, however, the integrand becomes nearly singular, though it is still Riemann integrable. A bigger imaginary part, which might allow us to evaluate the integral more easily, would certainly bring in another source of numerical error. For this reason it is sometimes argued that a simple sum like (2.9) will converge very slowly, if it ever converges. A critical check of the convergence is, therefore, to apply our integration scheme to a pure system. We first examine such a case in the following subsection and discuss the concentrated alloy cases later.

3.1. Pure limit

Pure Ni is a especially difficult test of our method since the density of states at E_F is high and strongly structured. Figure 1 shows the 'back-scattering' contribution (the second term of (2.17)) to the densities of minority (down) spin states at the Fermi level of Ni as a function of the number N of k-points. The remaining contribution (Green function for the single muffin-tin potential) to the densities of states are independent of N. An identical Ni potential is used for all cases. As was mentioned previously a small imaginary part, 10^{-4} (in au) in the present calculation, is attached to the Fermi level to avoid the divergences. The horizontal axis is scaled by N^2 for convenience.

Admittedly the convergence is not fast in this limit. However, the fluctuations observed for large N remain still small compared with the total density of states (about 23 states Ryd^{-1}/atom) which is obtained by adding the single potential contributions to the present 'back-scattering' ones.

The situation is completely different for quantities where in addition to the k-space integration also an energy integration is involved, such as charge and spin densities. In this case the integrand for the k-space integration contains only step-like functions even for real energies. This makes the convergence much better. Figure 2 shows the calculated magnetic moment of pure Ni for various $\{\boldsymbol{k}_n\}$ as a function of the number

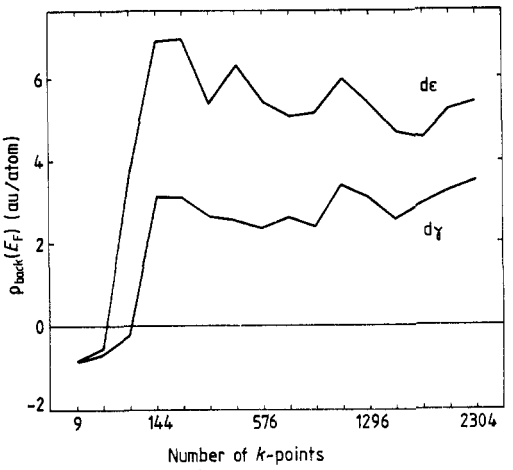

Figure 1. The 'back-scattering' contribution (see text) to the densities of down (minority) spin states at the Fermi level of Ni as a function of the number N of k-points. The horizontal axis is scaled by N^2.

N of k-points. The energy integral was performed along a complex energy path in the upper half plane. It started from sufficiently below the bottom of the band, going along a semielliptical circle, and ended at the Fermi level with a small imaginary part. It is shown that the integration converges fast without any noticeable fluctuation for N greater than about 300.

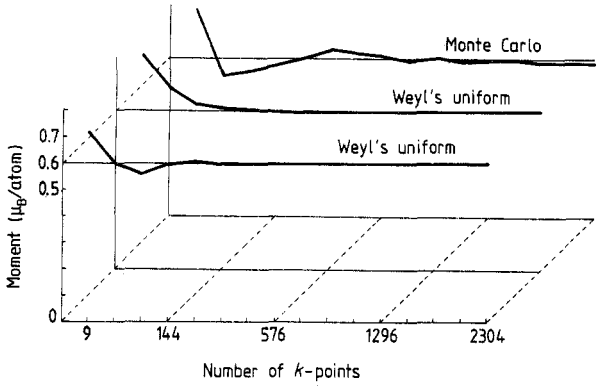

Figure 2. Calculated magnetic moments of Ni for various $\{k_n\}$ as a function of the number N of k-points. Results obtained by two different Weyl's distributions, one of them starting from $n = 1$ of (2.8) and the other from $n = 2000$, and that obtained by the Monte Carlo sampling are displayed. The horizontal axis is scaled by N^2.

A similar method of numerical integration is the Monte Carlo method. Though we did not use it in actual calculations because of its slower convergence, as was mentioned in §2, it is worthwhile comparing numerically the Monte Carlo integration method with our method of using Weyl's uniform distribution; the former, exhibiting a typical $1/\sqrt{N}$ fluctuation, is also given in figure 2. All results are given in table 1. We conclude that the number of k-points sufficient for a reliable results for, at least, the magnetic moment (due to its relatively small value this is already a difficult quantity in Ni) is as small as about 100.

Table 1. Calculated magnetic moments (μ_B/atom) of Ni with a frozen potential for various $\{\boldsymbol{k}_n\}$ as a function of the number N of k-points. Here 'Weyl I' corresponds to the series given by (2.8) with $N = (\sqrt{3}a, \sqrt{5}a, 2\sqrt{13}a)$, where $a = 0.359$, and $n = 1, 2, \ldots$ (see text), whereas 'Weyl II' corresponds to that with $n = 2000, 2001, \ldots$. The result obtained by the Monte Carlo sampling is denoted by MC.

	Magnetic moment (μ_B/atom)		
N	Weyl I	Weyl II	MC
9	0.725	0.811	0.778
36	0.593	0.686	0.539
81	0.562	0.628	0.550
144	0.599	0.607	0.577
225	0.614	0.607	0.602
324	0.604	0.605	0.639
441	0.607	0.597	0.622
576	0.604	0.596	0.615
729	0.601	0.594	0.600
900	0.599	0.594	0.604
1089	0.600	0.593	0.592
1296	0.599	0.595	0.595
1521	0.597	0.597	0.595
1764	0.597	0.594	0.588
2025	0.597	0.595	0.588
2304	0.597	0.597	0.587

It must be noticed that any quantities related to the ground state properties of the metallic systems are obtained through energy integrations. In other words, only such quantities can be true ground state properties in a sense of the density functional theory. For this reason our results showing good convergence for the magnetic moment, which is a typical ground state property, are quite satisfactory.

3.2. Alloy cases

In this subsection we examine the convergence of the iteration procedure (2.10)–(2.12) for concentrated alloys. Figure 3 shows the coherent t-matrices at the Fermi level E_F of the minority spin states of $Ni_{0.8}Fe_{0.2}$ as a function of the number of steps N of the procedure (2.10)–(2.12). Here only $d\varepsilon$ and $d\gamma$ components are displayed since others (s and p components) are virtually unchanged with increasing N for the present system. In general the convergence of the coherent t-matrix is slowest at the Fermi level for the same reason as discussed previously. Our calculation, nevertheless, shows fast enough convergences. From figure 3 it is concluded that around 300 k-points are sufficient to ensure converged results.

More difficult quantities may be the densities of states at the Fermi level. Though physically less transparent than energy-integrated quantities, those quantities given at the Fermi level are still interesting since they contain approximate information about low lying excitation of the system. Figure 4 shows the densities of minority spin states at the Fermi level plotted in a similar way as the coherent t-matrices. Again only the 'back-scattering' contributions to the density of states are considered. For this case a choice of the parameter α which controls the weighting factor (2.16) becomes important. In other words a bad history brought in at an early stage of the iteration procedure will, if the weighting factor is omitted, affect the densities of states considerably even

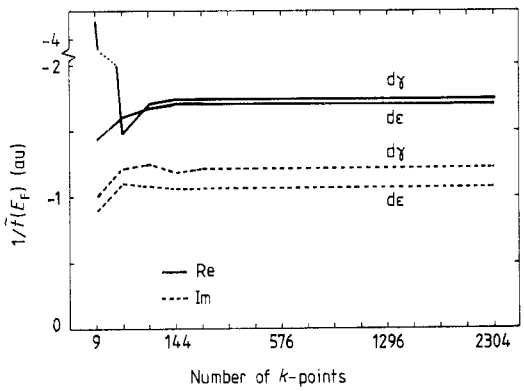

Figure 3. Coherent t-matrices at the Fermi level of down (minority) spin states of $Ni_{0.8}Fe_{0.2}$as a function of the number of steps N of the procedure given by (2.10)–(2.12). Only dε and dγ components are displayed. The horizontal axis is scaled by N^2.

after many iteration cycles have been repeated. We found that we should use $\alpha > 0.97$ to ensure the convergence within a reasonable number of iteration steps. However, the convergence of the coherent t-matrices is much less affected by the choice of the weighting factor.

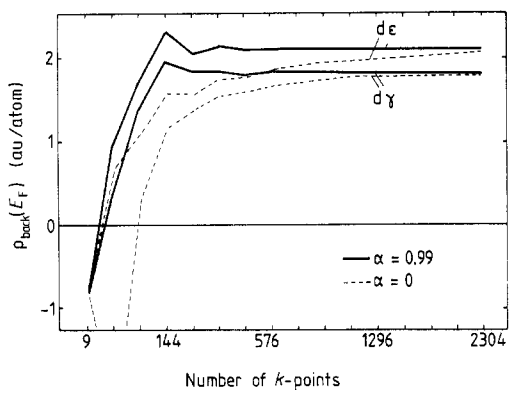

Figure 4. The 'back-scattering' contribution to the densities of down (minority) spin states at the Fermi level of $Ni_{0.8}Fe_{0.2}$ as a function of the number of steps N of the procedure given by (2.10)–(2.12) for $\alpha = 0$ and 0.99 (see text). The horizontal axis is scaled by N^2.

Finally we examine the total convergence of the whole procedure, i.e., KKR CPA plus LSD. Again we take the $Ni_{0.8}Fe_{0.2}$ system as an example. Figure 5 shows the calculated total magnetic moment. Now the self-consistent determination of both the coherent t-matrices and the potentials were performed. The calculations were performed for every $N = 9n^2$ with $n = 2,\ldots,16$. Each calculation, which started from atomic potentials, required around 30–50 big LSD iteration cycles for charge and magnetisation self-consistency with Chebyshev acceleration [24]. Final RMS errors in charge (spin) densities thus attained become less than 10^{-6} (in au). It might be worth noticing that the convergence with respect to N is now even better than with a fixed potential; the self-consistent determination of the potential during the iteration process automatically corrects for errors occurring, for example, in a frozen potential

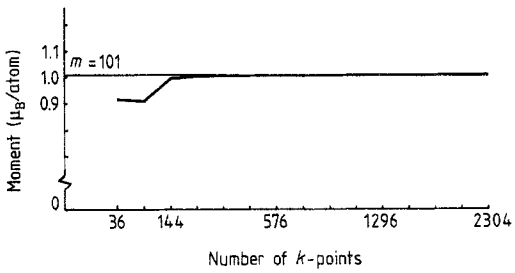

Figure 5. Calculated total magnetic moment as a function of the number of steps N of the procedure given by (2.10)–(2.12). The self-consistent determination of both the coherent t-matrices and the potentials are performed.

calculation. We conclude that our method with $N \simeq 300$–500 is enough for most practical purposes.

4. Electronic structure of the Ni–Fe system

This system was first dealt with by Hasegawa and Kanamori [25] within the framework of the tight-binding CPA combined with the Hartree–Fock approximation. The local magnetic moment as well as the saturation magnetisation and the electronic specific heat coefficient were discussed successfully by these authors. Later KKR CPA, without potential self-consistency, was applied to the same systems and the transport properties were discussed by the present author [11]. A full self-consistent calculation, KKR CPA LSD, was first performed for $Ni_{0.65}Fe_{0.35}$ by Johnson, Pinsky and Stocks [13]. More intensive calculations on this system have been performed by the present author; brief reports are given elsewhere [14, 15]. A similar calculation also has been reported by Pinsky, Staunton and Johnson [26].

In this section we demonstrate the application of our fast KKR CPA LSD method to this standard magnetic alloy. Figure 6 shows the change of the total energy with varying the lattice constant a of $Ni_{0.8}Fe_{0.2}$. We adopt the expression for the total energy which was given by Janak [27] for pure metals and was adapted to disordered alloys by Johnson *et al* [28]. The core contribution to the total energy is rigorously included. The energy origin of the structural Green function is shifted by +0.1 Ryd to avoid the zero of the p components of the t-matrix (see §2.2), which happens at the Fermi level for a certain concentration range. (We found later that this value could be much smaller in absolute terms, e.g. +0.01 Ryd, for the present systems; the calculation would predicts a slightly (0.12%) smaller value for the equilibrium lattice constant in that case.) We use $N = 500$ and $\alpha = 0.99$ for the iteration procedure. From this figure we determined the equilibrium lattice constant of $Ni_{0.8}Fe_{0.2}$ in the present calculation to be $a = 6.624$ (in au).

A similar calculation for $Ni_{0.5}Fe_{0.5}$ is performed to demonstrate the dependence of the equilibrium lattice constant on N, as is shown in figure 7. Four different values of N (N=500, 800, 1000, 1200) are used to calculate the total energy. Since the difference in the total energy among them is much bigger than the systematic change in the total energy with varying the lattice constant, each curve is arbitrarily shifted so that the direct comparison of the position of the relative minima of the total energy among them becomes possible. From this figure we conclude that the ambiguity in the lattice

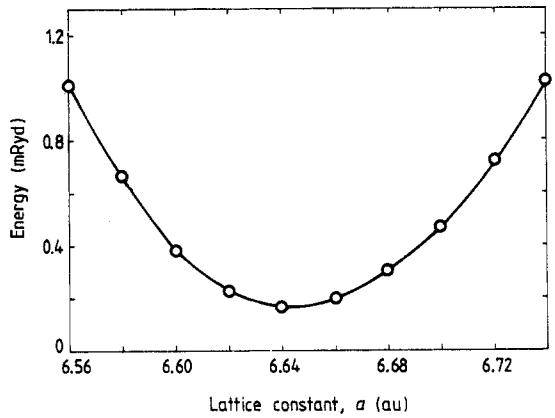

Figure 6. Change of the total energy with varying the lattice constant of $Ni_{0.8}Fe_{0.2}$.

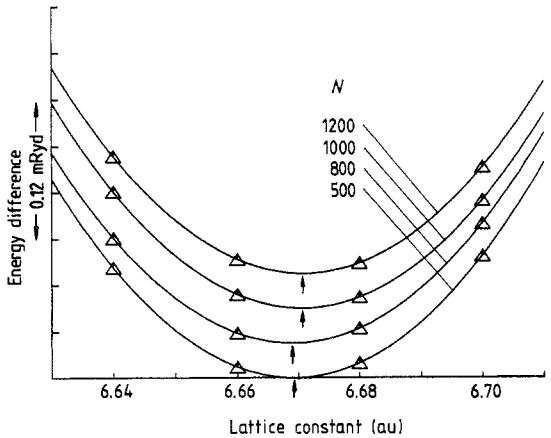

Figure 7. Total energy of $Ni_{0.5}Fe_{0.5}$ versus lattice constant for different N (N: the number of k-points). A small dependence of the equilibrium lattice constant (shown by ↑) on N is demonstrated. Each curve is shifted so that the direct comparison among them is possible.

constant obtained in our method is less than 0.03 %, which of course is much smaller than the ambiguity coming from the LSD approximation, and may be safely neglected.

In figure 8 we show the band structure of $Ni_{0.8}Fe_{0.2}$ along the ΓX line. Here we plotted a spectral function $A(E,\boldsymbol{k})$ defined by

$$A(E,\boldsymbol{k}) = -\frac{1}{\pi}\,\mathrm{Im}\frac{\mathrm{d}Z(E,\boldsymbol{k})}{\mathrm{d}E} \tag{4.1}$$

where

$$\begin{aligned} Z(E,\boldsymbol{k}) = {} & \ln\det\left[-E+(\boldsymbol{k}+\boldsymbol{g})^2\right] + \ln\det\left(t^{-1}-G_0\right) \\ & + c_{\mathrm{A}}\ln\det\left[1+T(t_{\mathrm{A}}^{-1}-t^{-1})\right] + c_{\mathrm{B}}\ln\det\left[1+T(t_{\mathrm{B}}^{-1}-t^{-1})\right] \end{aligned} \tag{4.2}$$

measures the total number of states below the real energy E. In order to make such plots possible even for weak scattering limits, where the spectrum shows δ-function-like spikes, we attached a rather big imaginary part 10^{-3} (in au) to the real energies. Figure 9 shows the total and component (partial) densities of states. The component densities

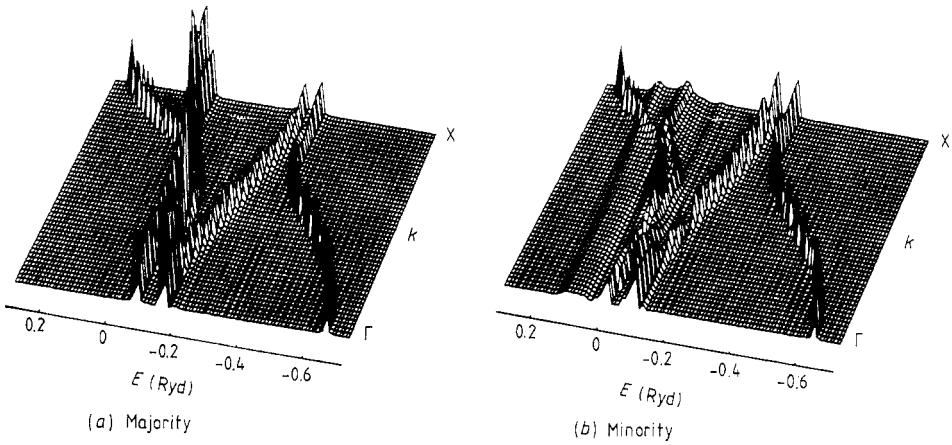

Figure 8. Three-dimensional plots of the band structure of $Ni_{0.8}Fe_{0.2}$ along the ΓX line for (*a*) the majority and (*b*) the minority spin states. The spectral functions $A(E, k)$ defined by (4.1) are plotted. A rather big imaginary part 10^{-3} (in au) is attached to the real energies.

of states are calculated inside the muffin-tin sphere at each site. Note that the total density of states here is not an average densities of states of the component densities of states but that obtained directly from the *k*-space summation of (2.9). As was pointed out by Hasegawa and Kanamori [25], the alloying effects are pronounced only for the down (minority) spin band. For the up (majority) spin band the difference between Ni and Fe occurring in the Hartree potentials is almost cancelled by the difference in the local exchange splitting. Therefore figure 8(*a*) shows essentially the same unperturbed majority band structure as pure Ni, whereas the minority band is strongly broadened in the vicinity of the Fe resonance. The calculated saturation magnetisation is 1.01 μ_B/atom and the local magnetic moments are 0.64 and 2.54 μ_B for Ni and Fe sites, respectively.

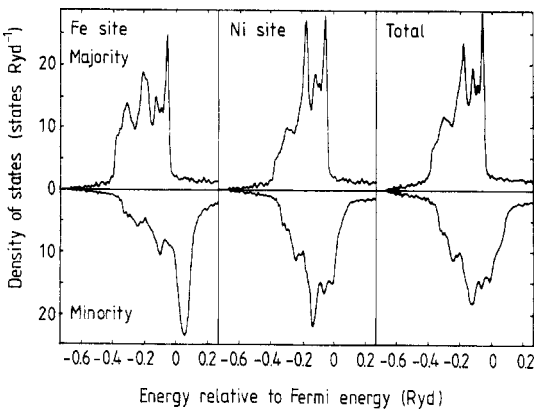

Figure 9. Total and component densities of states of $Ni_{0.8}Fe_{0.2}$. The component densities of states are those calculated within the muffin-tin sphere at each site. The total densities of states are obtained by the direct *k*-space summation of (4.2) and hence include the contributions from both inside and outside the muffin-tin sphere as well as some of the contribution from higher angular momenta.

Finally we show the concentration dependence of the lattice constant, the total

and local magnetic moments, the hyperfine fields and the Mössbauer isomer shifts of $Ni_{1-x}Fe_x$ systems. Some discussions of the results, especially in connection with the Invar alloy, are given elsewhere [29].

Figure 10 shows the concentration dependence of the lattice constant. It constantly increases with increasing Fe concentration. The main reason of this volume expansion lies in the similar increase of the total magnetic moment (see the magnetisation shown in figure 11). In other words, an Fe atom has a bigger volume than a Ni atom because of the bigger local magnetic moment of the Fe atom (figure 11), and hence, replacing Ni atoms by Fe atoms causes a volume expansion. Another possible source of the volume expansion is an alloying effect. However, since non-magnetic Fe has a smaller atomic volume than Ni [3], we naturally expect a volume contraction if the system is kept non-magnetic. From this we conclude that the magnetic effect dominates the equilibrium lattice constant for this system. Comparing the present result with experiments, we may say the calculation well explains the trends of concentration dependence of the lattice constant except in the Invar region (see below).

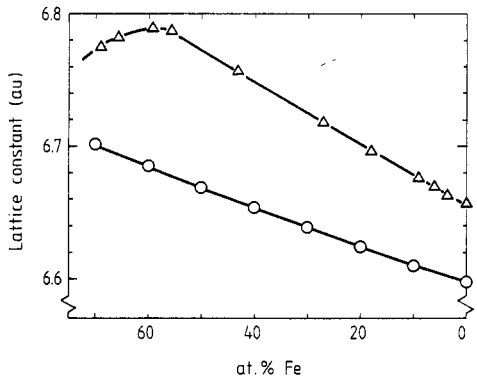

Figure 10. The equilibrium lattice constant of Ni–Fe as a function of Fe concentration. Open circles: calculated results; open triangles: experimental results

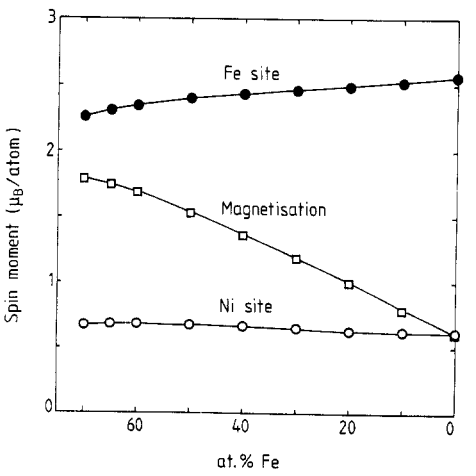

Figure 11. Calculated local magnetic moments at Ni and Fe sites and the magnetisation of Ni–Fe.

For $x \simeq 0.7$ we obtain two stable solutions for the system, one ferromagnetic and the other non-magnetic. Each of these states has a different lattice constant as is seen in figure 12, which plots the total energy of $Ni_{0.3}Fe_{0.7}$ as a function of the lattice constant; the non-magnetic state has lower energy in this case. We thereby expect that a first-order transition from ferromagnetic to non-magnetic state take place at a certain concentration near $x = 0.7$. This seemingly contradicts experimental observation which shows a rather moderate transition. For this point, we suggested that either our treatment is oversimplified or the experimental situation is different from what is normally assumed [29]. We give further details in [29].

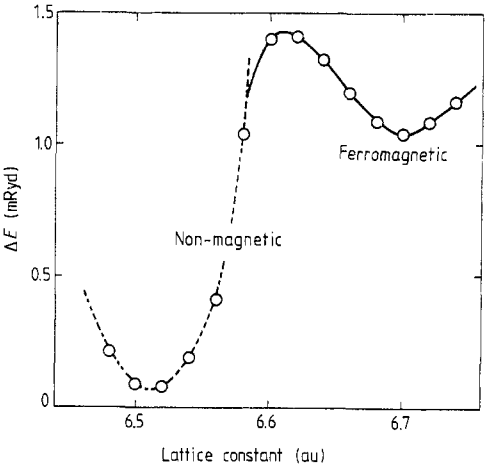

Figure 12. Total energy versus lattice constant for $Ni_{0.3}Fe_{0.7}$. Two local minima correspond to the equilibrium lattice constant of non-magnetic ($\simeq$ 6.52 (in au)) and ferromagnetic ($\simeq$ 6.70 (in au)) states, respectively. Note that the path along the ferromagnetic state does not join smoothly to that along the non-magnetic state.

The hyperfine fields at Ni and Fe nuclei are shown in figure 13. As is well known, the experimental hyperfine field of Fe can not be well reproduced by calculation based on LSD [20, 30]. For this reason, we have to restrict ourselves to a discussion of the general trends. The hyperfine fields of both the Ni and Fe site increase in absolute with increasing Fe concentration. This is due to the increase of the magnetisation which enhances the negative polarisation at the nuclear position produced by tail parts of d wavefunctions centred on the neighbouring sites (transfered contribution) [20, 30]. For transition elements another important contribution to the hyperfine field arises from local exchange splitting which, roughly speaking, is proportional to the local magnetic moment (local contribution). In the present case, however, this effect is not of primary importance for the overall trends because the local magnetic moments rather weakly depend on Fe concentration, especially for Ni atoms, whereas the magnetisation increases more than a factor two. For Fe, the decrease in the local magnetic moment with increasing Fe concentration, leading to a smaller local contribution to the hyperfine field, partly cancels the larger transfered contribution. The agreement of the present results with experiments is fairly good as far as the concentration dependence of the hyperfine fields is concerned. Some discrepancies seen at the critical region where the ferromagnetic state becomes unstable ($x > 0.6$) are related to the failure of the present treatment in this region, mentioned in the last paragraph.

From a numerical point of view, calculation of the Mössbauer isomer shift may

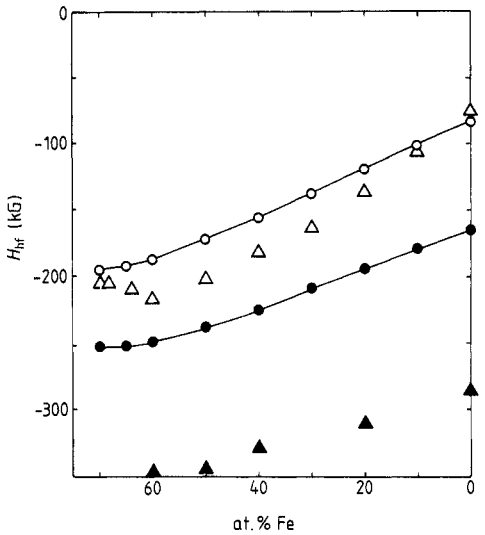

Figure 13. Concentration dependence of the hyperfine fields of Ni–Fe system. Open circles: calculated results for the Ni site; full circles: calculated results for the Fe site; open triangles: experimental results for the Ni site; full triangles; experimental results for the Fe site.

provide the most critical check of the accuracy since it counts a small deviation, which amounts only to one part of 10^6, of the charge density at the nuclear position. The present calculation gives (figure 14) a fairly smooth curve without any scattered points for the concentration dependence of the isomer shift, proving its reliability. Because of their experimental importance, we only give the calculations for Fe nucleus in figure 14. It decreases with increasing Fe concentration, implying that the charge density at the nuclear position increases. From a general discussion developed previously for the isomer shift of impurity systems [32], we expect that it is a directly reflection of the increase in the valence s charge. Since no experimental data are available by now, it is highly desirable to have experimental data for Ni–Fe systems in order to check the theoretical results.

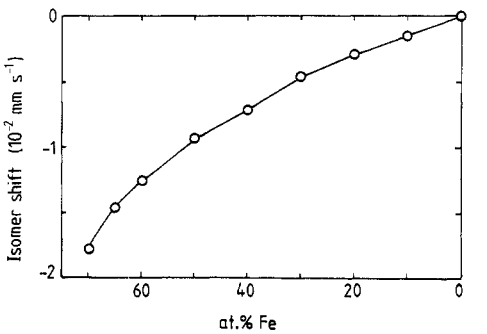

Figure 14. Concentration dependence of Fe isomer shift of Ni–Fe system. The isomer-shift calibration constant of $\alpha = -0.24a_0^3$ mm s^{-1} is used following a similar calculation for impurity systems (see [32]).

We will not discuss the electronic structure of this system in further detail because it is not our principal aim here. We only stress that our apparently crude method of

solving the CPA problem actually turns out to be sufficiently accurate for calculating many physical quantities which are otherwise very difficult to deal with for disordered systems.

5. Summary

A fast KKR CPA method has been explained in detail. The convergence properties of the procedure used in the method are fully examined numerically. It is shown that a step number of $N \simeq 300$–500, which determines the number of the k-points used for the numerical integration as well as the number of iteration steps in determining the coherent t-matrix, is sufficient for most purposes, including total-energy calculations.

Some other techniques which generally improve the convergence, for instance the introducing of the weighting factor, are also presented. The method is applied to $Ni_{1-x}Fe_x$ systems to demonstrate how it works. The calculated total energy versus lattice constant curve, the band structure, the densities of states are all quite reasonable in comparison with the corresponding calculation for pure systems. The concentration dependence of the lattice constant, the local and the total magnetic moments, the hyperfine fields and the isomer shift have been also calculated with reasonable agreements with existing experimental data.

Our observation obtained through those numerical tests is the following. First, our k-space summation is much better than one might think and, second, the remaining inaccuracy originating from, say, the small number of the sampling points after all does not degrade the results because of the self-correcting properties of the iteration process.

In conclusion our numerical technique together with the rapid development of supercomputers makes KKR CPA LSD calculations really fast. A typical supercomputer can run each big LSD iteration cycle in 1–1.7 cpu s with our fast KKR CPA method (with 500 k-points), which compares very well with the usual band structure calculations for ordered systems. Thus KKR CPA LSD calculations are not more time consuming than normal band structure calculations, if the present methods are used. Finally we point out that our method is applicable to a large class of problems where a numerical integration for an integrand with unknown parameters which have to be determined self-consistently is necessary.

Acknowledgments

I am grateful to Professor P H Dederichs and Professor J Kanamori for their valuable discussions. The cordial hospitality of the Institut für Festkörperforschung der Kernforschungsanlage Jülich, where a large part of the present calculations were performed, is greatly appreciated. I also would like to thank Dr T Irisawa of Gakushuin University for kindly offering computer graphic codes. This work is partly supported by Grant-In-Aid for Scientific Research from the Japanese Ministry of Education, Science and Culture.

References

[1] Shiba H 1971 *Prog. Theor. Phys.* **46** 77
[2] Soven P 1970 *Phys. Rev.* **B2** 4715

[3] Moruzzi V L, Janak J F and Williams A R 1978 *Calculated Electronic Properties of Metals* (New York: Pergamon)
[4] Akai H 1982 *J. Phys. Soc. Japan* **51** 468
[5] Jo T and Akai H 1981 *J. Phys. Soc. Japan* **50** 70
[6] Winter H and Stocks G M 1983 *Phys. Rev.* B **27** 882
[7] Winter H, Durham P J, Temmerman W M and Stocks G M 1986 *Phys. Rev.* B **33** 2370
[8] Johnson D D, Pinsky F J and Stocks G M 1985 *J. Appl. Phys.* **57** 3018
[9] Akai H 1989 *Mater. Sci. Forum* **37** 211
[10] Kanamori J and Akai H 1989 *Mater. Sci. Forum* **37** 1
[11] Akai H 1977 *Physica* B **86–88** 539
[12] Akai H and Kanamori J 1982 *J. Phys. Soc. Japan* **51** 1176
[13] Bansil A 1978 *Phys. Rev. Lett.* **41** 1670
[14] Stocks G M, Temmerman W M and Gyorffy B L 1978 *Phys. Rev. Lett.* **41** 339
[15] Stocks G M and Winter H 1982 *Z. Phys.* B **46** 95
[16] Beeby J L 1967 *Proc. R. Soc.* A **302** 113
[17] Harris R 1972 *J. Phys. C: Solid State Phys.* **3** 172
[18] Hamazaki M, Asano S and Yamashita J 1976 *J. Phys. Soc. Japan* **41** 378
[19] Podloucky R, Zeller R and Dederichs P H 1980 *Phys. Rev.* B **22** 5777
[20] Akai M, Akai H and Kanamori J 1985 *J. Phys. Soc. Japan* **54** 4246; 1985 *J. Phys. Soc. Japan* **54** 4257; 1987 *J. Phys. Soc. Japan* **54** 1064
[21] Zeller R, Deutz J and Dederichs P H 1982 *Solid State Commun.* **44** 993
[22] Haselgrove C B 1961 *Math. Comput.* **15** 323
[23] Andersen O K 1973 *Solid State Commun.* **13** 133
[24] Akai H and Dederichs P H 1985 *J. Phys. C: Solid State Phys.* **18** 2455
[25] Hasegawa H and Kanamori J 1971 *J. Phys. Soc. Japan* **31** 382; 1972 *J. Phys. Soc. Japan* **33** 1599; 1972 *J. Phys. Soc. Japan* **32** 1607
[26] Johnson D D, Pinsky F J and Staunton J B 1987 *J. Appl. Phys.* **61** 3715
[27] Janak J F 1974 *Phys. Rev.* B **9** 3985
[28] Johnson D D, Nicholson D M, Pinsky F J, Gyorffy B L and Stocks G M 1986 *Phys. Rev. Lett.* **56** 2088
[29] Akai H, Dederichs P H and Kanamori J 1988 *J. Physique* C **8** 23
[30] Blügel S, Akai H, Zeller R and Dederichs P H 1987 *Phys. Rev.* B **35** 2407
[31] Akai H, Blügel S, Zeller R and Dederichs P H 1987 *Phys. Rev. Lett.* **56** 2407